LANGMUIR

pubs.acs.org/Langmuir Article

Designing Multicomponent Polymer Colloids for Self-Stratifying Films

Piyush K. Singh, Michaeleen L. Pacholski, Junsi Gu, Yoo Kyung Go, Gaurav Singhal, Cecilia Leal, Paul V. Braun, Kshitish A. Patankar, Ray Drumright, Simon A. Rogers, and Charles M. Schroeder*

Cite This: *Langmuir* 2022, 38, 11160−11170 Read Online

ACCESS | Metrics & More | Article Recommendations | Supporting Information

ABSTRACT: Aqueous polymer colloids known as latexes are widely used in coating applications. Multicomponent latexes comprised of two incompatible polymeric species organized into a core−shell particle morphology are a promising system for self-stratifying coatings that spontaneously partition into multiple layers, thereby yielding complex structured coatings requiring only a single application step. Developing new materials for self-stratifying coatings requires a clear understanding of the thermodynamic and kinetic properties governing phase separation and polymeric species transport. In this work, we study phase separation and self-stratification in polymer films based on multicomponent acrylic (shell) and acrylic−silicone (core) latex particles. Our results show that the molecular weight of the shell polymer and heat aging conditions of the film critically determine the underlying transport phenomena, which ultimately controls phase separation in the film. Unentangled shell polymers result in efficient phase separation within hours with heat aging at reasonable temperatures, whereas entangled shell polymers effectively inhibit phase separation even under extensive heat aging conditions over a period of months due to kinetic limitations. Transmission electron microscopy is used to track morphological changes as a function of thermal aging. Interestingly, our results show that the rheological properties of the latex films are highly sensitive to morphology, and linear shear rheology is used to understand morphological changes. Overall, these results highlight the importance of bulk rheology as a simple and effective tool for understanding changes in morphology in multicomponent latex films.

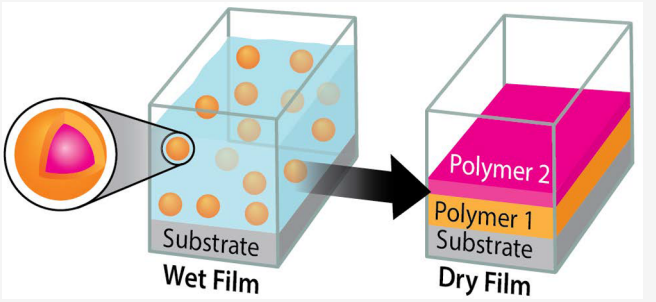

1. INTRODUCTION

Latexes are aqueous polymer colloids commonly used in household paints, varnishes, pressure-sensitive adhesives, textiles, carpet backings, paper coatings, and inks. Waterborne latex particles and films offer sustainable routes for smart coating systems by minimizing or avoiding organic solvents during formulation and processing. In recent decades, significant progress has been made in understanding the fundamental physics governing the film-forming process in latex coatings.[1−9]

Film formation for a single-component latex (comprising one polymer or copolymer chemistry with possible polydispersity in chain length and particle size) typically progresses as a sequence of three steps: (1) water evaporation and film drying leading to close-packed polymer particles, (2) particle deformation during solidification, and (3) interdiffusion of polymer chains across particle boundaries, resulting in coalescence and formation of a continuous film. In reality, these steps occur simultaneously and the processes are interrelated.[10−14] Interdiffusion is a critical step in film formation, wherein polymer chains diffuse into neighboring particles leading to the energetically favorable continuous films (reduced surface area) with enhanced mechanical strength. Pioneering work in this area[1−9] demonstrated that interdiffusion is governed by reptation dynamics for entangled polymer chains.[15−21] Particle deformation and interdiffusion in steps 2 and 3 occur for soft latex particles, where the application temperature is maintained above the polymer glass transition temperature (T_g). For lower application temperatures, a powdery and brittle film is formed.

In contrast to single-component latex particles, multicomponent latex particles are comprised of two distinct polymeric species such as a core−shell particle. Films from multicomponent latexes can be tailored for enhanced performance by modulating the properties and composition of individual polymer components.[22] For example, the addition of a high-T_g component can enhance the strength of a low-T_g film forming latex. Although similar properties can be achieved for a blend of single-component latexes, multicomponent

Received: April 2, 2022
Revised: August 20, 2022
Published: September 2, 2022

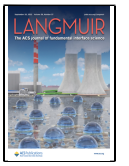

https://doi.org/10.1021/acs.langmuir.2c00855
Langmuir 2022, 38, 11160−11170

latexes allow for enhanced control of film morphology because both polymers are contained in a single particle.[23] In addition, prior work has shown that a blend of latex particles can show distinctly different segregation based on the relative particle sizes and rates of evaporation.[24−26]

Multicomponent latexes allow for formation of self-stratified films, which is an attractive feature for the development of new functional coatings (Figure 1). Despite recent progress, we lack a complete understanding of the thermodynamics and kinetics governing the self-stratification process during film formation. From a thermodynamic perspective, a multicomponent latex film comprised of incompatible polymers is predicted to phase separate into an energetically favorable state with two distinct polymer matrix layers. The surface-adjacent layer (with a larger surface energy) can be tailored to provide strong adhesion to the substrate, whereas the air-adjacent layer (with a smaller surface energy) can be designed with water-, fire-, ultraviolet-, or microbial-repellent properties depending on the desired application. However, the process of self-stratification can be kinetically or chemistry limited due to several factors. As water evaporates, the colloidal particles (shells) come into contact and coalesce via interdiffusion to form a continuous matrix embedding the polymeric core phase. The incompatibility of core polymers with a shell matrix drives coalescence and phase separation. However, the process of core species diffusion can be kinetically limited because the shell matrix is typically highly viscous, effectively resulting in hindered diffusion of core polymer species in the shell matrix. Even if the core polymer species is sufficiently mobile for coalescence, the surface energy difference and/or immiscibility between the two polymers might not be large enough to drive separation into two distinct layers, resulting in co-continuous domains similar to those frequently observed for polymer solution blends.[27] We show two such extreme intermediate cases of individual core spheres and full coalescence of core spheres into a single domain in Figure 1. In broad terms, however, there can be a wide range of intermediate steps depending on the varying degree of kinetic limitations including a zebra-stripe structure in which fewer spheres coalesce in separate locations to give multiple core domains. For the sake of simplicity, we show only two kinetically hindered intermediate states. In addition, prior work on self-stratifying multicomponent latex films was primarily focused on specific polymer chemistries, providing differing results for self-stratification depending on the choice of polymer chemistry.[28−31] In some cases, prior reports focused on characterizing the concentration profiles near the air−film and film−substrate interfaces while reporting self-stratification behavior.[32] However, nonmonotonic concentration profiles of the underlying phases across the entire film depth cannot be excluded due to complexities in the phase separation process.

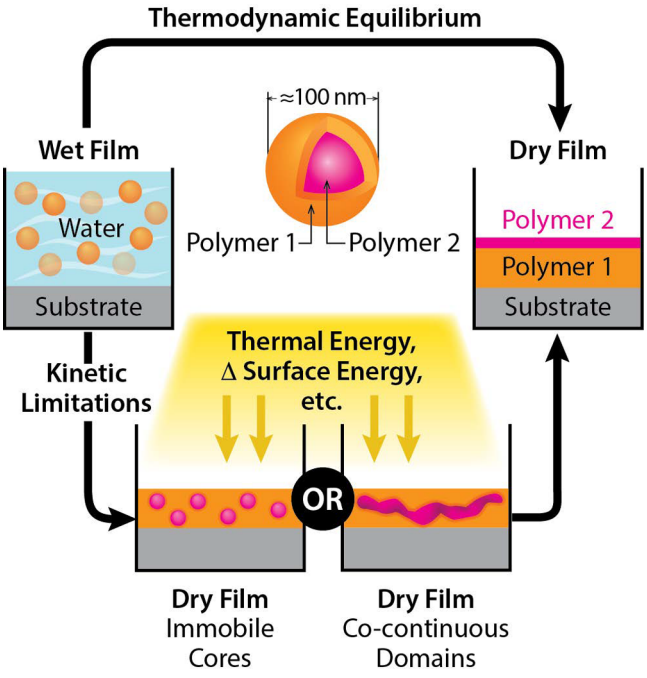

Figure 1. Multicomponent latexes as a self-stratifying coating system. A thermodynamically preferred state of the dried film shows a distinct two-layer structure. As a first step, the shells come into contact, and the shell polymer chains interdiffuse across particle boundaries, resulting in a continuous shell matrix around the cores. The incompatibility or immiscibility of the polymers drives the core spheres to diffuse toward each other, coalesce, and form a continuous matrix of the core polymer. If the surface energies of the polymers are significantly different, then the high-surface energy polymer matrix would prefer to be at the film−substrate interface whereas the lower-surface energy component would prefer to be at the air−film interface. However, this process can be kinetically limited and could potentially be halted at any of the intermediate steps. We show two extreme intermediate cases of individual core spheres and full coalescence of core spheres into a single domain. Although we show only these two intermediate cases, in broad terms, there can be a wide range of intermediate steps including a zebra-stripe structure in which fewer spheres coalesce in separate locations to give multiple core domains.

In this work, we study the self-stratifying properties of films formed from multicomponent latex particles by varying both the molecular weight (M) of the shell polymer and the heat aging conditions of the dry film. In particular, we consider multicomponent acrylic (shell) and acrylic−silicone (core) latex particles, which provides a system with sufficiently incompatible polymer chemistries to drive phase separation. Two regimes of polymer molecular weight are considered: unentangled and entangled shell polymers. Our results show that the molecular weight of the shell polymer and heat aging conditions are critical parameters dictating the kinetics of polymer phase separation in multicomponent latex films. Bulk rheology is used to characterize film properties and microstructure, whereas alternative methods such as small-angle X-ray scattering (SAXS) and secondary ion mass spectrometry (SIMS) were found to be insufficient to fully characterize film morphology. Broadly, these results highlight the importance of characterization methods for studying multicomponent latex film morphology for the development of self-stratifying films.

Note that multicomponent latex particles are synonymously called multiphase latex particles,[33] composite latex particles,[34] or polymer−polymer hybrid latex particles.[10] In this work, we will retain the nomenclature "multicomponent latex particle", implying a latex particle comprised of two distinct polymeric species.

The main objective in this work is to understand self-stratification in film-forming colloidal particles, which differs from related studies on structural characterization in hard sphere colloidal suspensions. Colloidal suspensions show a rich variety of structures in their dispersed state depending on particle size, polydispersity, and surface charges.[35−41] In addition, colloidal particles can be patterned into various complex structures after carrier fluid evaporation depending on the nature of the substrate, particle properties, and interparticle

https://doi.org/10.1021/acs.langmuir.2c00855
Langmuir 2022, 38, 11160−11170

Table 1. Weight Average Molecular Weights, Particle Sizes, and Relative Weight Percentages of Species in Latex Suspensions

	shell (acrylic)		core (acrylic−silicone)				
polymer	M	$Đ$	M	$Đ$	particle size (nm)[a]	wt % of core in latex particle	wt % of solids in suspension
CS-L	18.9 K	1.8	369.0 K	1.5	110.0	26.0	32.8
CS-H	262.8 K	4.5	369.0 K	1.5	134.4	17.4	31.6
S-L	18.9 K	1.8	–	–	110.0	–	43.0
S-H	262.8 K	4.5	–	–	117.6	–	46.0

[a]Determined via dynamic light scattering (DLS).

interactions.[42,43] Although such patterned colloidal structures are technologically relevant,[44−57] in this work, we are mainly focused on understanding the film formation and self-stratification process, rather than quantifying the evolution of the colloidal suspension structure during solvent evaporation. Film-forming soft latex particles typically lose their discrete particle identity upon coalescence, which facilitates film formation on a substrate. In this work, we are primarily interested in understanding the evolution of film morphology in terms of the polymeric constituent in the core−shell particles. Related systems based on spin-coated polymeric films consisting of two incompatible polymers dissolved in a common solvent have also been studied.[58] Although the interaction forces driving film morphology in multicomponent latexes and incompatible polymer solutions are similar, the kinetic evolution of film morphology is qualitatively different in these two systems. In an incompatible polymer solution, the two polymers begin to phase separate in the solution phase, whereas for multicomponent latexes, any putative phase separation occurs during or after the evaporation of solvent. Overall, waterborne latex suspensions are typically preferred for coatings and paint applications.

Our work also shows some key distinctions compared to prior studies on evaporative self-assembly of colloidal particles.[24−26,59,60] For evaporation rates much larger than the diffusion rate of colloidal particles, i.e., Peclet number $Pe > 1$, colloidal particles tend to cluster at the air−film interface. The particle clustering effect has been pursued for blends of different sized colloids, where different regimes of particle self-stratification, for example, larger particles segregating into regions above regions of smaller particles (or vice versa), are obtained depending on the Pe, relative volume fractions of different sized particles, and electrostatic interactions.[24,61−66] If one or both of the components are polymer latexes, a film with a self-stratified structure is generally observed.[67,68] On the contrary, in our work, we focus on the design of a single multicomponent latex that results in self-stratification without the need for controlling evaporation rates or using polydisperse colloidal samples. Our work focuses primarily on enabling self-stratification during the later stages of solvent evaporation.

2. MATERIALS AND METHODS

2.1. Preparation and Characterization of Latex Particles. We studied two multicomponent latexes with acrylic as the shell polymer and acrylic−silicone (random copolymer) as the core polymer (Table 1). For both latexes, the molecular weight of the core polymer was held constant, but the molecular weight of the shell polymer was varied. The latex particles are denoted as CS-L and CS-H (CS for core−shell, L for lower-molecular weight shell polymer, and H for higher-molecular weight shell polymer). In addition, we studied two single-component latexes comprised of the two different molecular weight acrylic polymers. These latex particles are denoted as S-L and S-H, using a nomenclature scheme similar to that of multicomponent latexes.

Latex particles were synthesized by preparing a monomer pre-emulsion by homogenizing a mixture of water, surfactant (sodium lauryl sulfate), and monomer. A 2 L round-bottom flask equipped with an overhead stirrer, a condenser, a nitrogen inlet, and a thermocouple was charged with deionized water and surfactant. The thermal initiator was added, followed by a gradual addition of the monomer pre-emulsion. For multicomponent latexes, a second monomer pre-emulsion with a different composition was added sequentially. Upon addition of all of the remaining monomer, the residual monomer was reduced using a redox couple. Resulting latexes were characterized for molecular weights (M) and polydispersity ratios ($Đ$) of core and shell polymers, particle sizes from dynamic light scattering (DLS), and relative weight percentages of species in suspensions (Table 1).

The acrylic and acrylic−silicone species are blends of different polymeric species. In brief, the acrylic polymer is taken to be poly(methyl methacrylate) (PMMA) and the acrylic−silicone as a 1:1 (molar) copolymer of PMMA and poly(dimethylsiloxane) (PDMS). On the basis of the stoichiometry and materials property information provided in Table 1, the composition (mole percent) of Si in dry films is estimated to be ≈1% for CS-L and ≈0.68% for CS-H. The surface energy of the shell polymer assuming PMMA is taken to be 39 mN/m, whereas the surface energy of the core polymer taken as a blend of PMMA and PDMS is estimated to be 31.5 mN/m.[69]

Comparing the molecular weights of S-L and S-H with that of PMMA (M_e = 13.6 K)[70] yields an M/M_e of ≈1.39 for S-L, suggesting a weakly entangled (or unentangled) polymer, and an M/M_e of ≈19.3 for S-H, suggesting a well-entangled polymer, where M_e is the molecular weight between entanglements. The core polymer chains (acrylic−silicone copolymer) are expected to be well entangled because M = 369 K is an order of magnitude larger than the M_e of common acrylates such as PMMA (M_e = 13.6 K) and silicones such as PDMS (M_e = 12 K).[70]

2.2. Preparation of Latex Films. Latex films were drop-cast on piranha-cleaned glass slides for all experiments except SIMS, as described below. Samples were drop-cast and dried under ambient conditions ($T \approx 27.5$ °C) for thermogravimetric analysis (TGA) and differential scanning calorimetry (DSC). For shear rheology experiments, films were drop-cast inside stainless steel washers with a 25 mm inner diameter and a 1 mm thickness. Samples were dried for 3−6 days, and complete drying was confirmed by detection of no mass changes at 100 °C via TGA (Figure S1a−d). For heat aging, films were first completely dried under ambient conditions, followed by exposure to a vacuum oven at 75 °C for specified amounts of time. Dry sample discs were removed from glass slides with a razor blade for rheology, SAXS, and transmission electron microscopy (TEM). For SIMS, approximately 100 μm thick wet films were blade coated on 0.06 mm thick mylar sheets and dried under ambient conditions or heat aged in a vacuum oven at 75 °C for specified amounts of time.

2.3. Glass Transition Temperature of Latexes. The glass transition temperatures (T_g) of all four samples were determined via DSC by heat−cool−heat cycling. The inflection point of a second heat cycle was taken to be glass transition temperature T_g, which was found to be −0.83, 10.65, 0.53, and 12.42 °C for S-L, S-H, CS-L, and CS-H, respectively (Figure S2a−d). The multicomponent latexes displayed a single inflection point even with two polymer species, which was likely due to the proximity of the T_g's of the two polymer species.[33]

https://doi.org/10.1021/acs.langmuir.2c00855
Langmuir 2022, 38, 11160−11170

2.4. TEM Imaging of Latex Particles. Latexes were prepared via a two-stage emulsion polymerization,[71−76] where kinetic limitations may inhibit the desired core−shell particle morphology.[33,34,77] We therefore characterized latex particles using electron microscopy to assess the core−shell particle morphologies prior to film formation. TEM was performed in a Thermo Fisher Tecnai G2 Spirit BioTwin TEM instrument equipped with a LaB6 filament operating at 100 kV. The micrographs were recorded with a Gatan OneView camera. Latex particle samples were prepared by diluting two drops of a sample in 10 mL of distilled, deionized (DI) water and then nebulizing onto a plasma-treated Cu grid (200 mesh, Formvar/carbon support) at −75 °C. The holder temperature was maintained at −75 °C during imaging. To study particle morphology in the dry film, the suspension was first dried at room temperature for 48 h on an aluminum pin mount with a target thickness of 2 mm. The sample was then sectioned into 100 nm thin films at −80 °C in a Leica Ultracut EM UC7/FC7 cryo-ultramicrotome and transferred onto Cu grids (200 mesh, Formvar/carbon support). For studying the aged dry film morphology, sections were removed from dry sample discs. The imaging of the sections was performed at room temperature (≈27.5 °C) without staining.

2.5. Rheological Characterization of Latex Films. Rheology measurements were performed on a TA Instruments ARES-G2 rheometer. Small-amplitude oscillatory shear (SAOS) measurements were conducted over a wide range of temperatures, and master curves were obtained using time−temperature superposition (TTS).[78−80] A 25 mm parallel plate geometry was used with a serrated bottom plate to avoid potential slip at lower temperatures. Experiments were conducted inside a convection oven with a nitrogen gas flow to avoid sample oxidation. The temperature ranges used for TTS on various samples were 27.5−85 °C for S-L, 27.5−95 °C for CS-L, 27.5−140 °C for S-H, and 40−130 °C for CS-H. Thermal degradation of samples generally began in the vicinity of 150 °C as observed in TGA (Figure S1a−d), so the upper temperature was kept below 150 °C. At each temperature, SAOS experiments were performed in the angular frequency range of 0.1−100 rad/s and were limited to ∼15 min, which is well below the time scale for any morphological changes in the film (vide infra). A reference temperature of 27.5 °C was used to obtain SAOS master curves.

2.6. Small-Angle X-ray Scattering. Ex situ SAXS experiments in transmittance mode were performed at beamline 12-ID-B, Advanced Photon Source (APS), Argonne National Laboratory, using a Pilatus 2M detector for X-ray beam with an average photon energy of 13.3 keV. The sample-to-detector distance (SDD) was 3.61 m. The SDD calibration was performed using a silver behenate powder standard. The one-dimensional $I(q)$ plots were obtained by radially averaging two-dimensional scattering patterns upon acquisition.

2.7. Secondary Ion Mass Spectrometry. Time-of-flight secondary ion mass spectrometry (TOF-SIMS) data were acquired using an IONTOF V instrument (Munster, Germany). The analysis beam was a 30 keV Bi_3^+ beam in bunched mode. Sputtering was accomplished with a gas cluster ion beam (GCIB) operating at 10 kV with Ar_{1500}^+ clusters operating at a current of ∼11 nA. Charge compensation was used with a current of ≤2 μA. Then, 500 × 500 μm sputter craters were created in noninterlaced mode with analysis craters of 200 μm × 200 μm or 256 pixels × 256 pixels in a random raster mode in a 1 sputter frame/1 analysis frame/0.5 s pause cycle. The instrument cycle time was 200 μs. SurfaceLab 7.2.125120 was used for data analysis. Multiple analyses were performed on each sample to ensure sample homogeneity.

3. RESULTS AND DISCUSSION

We began by characterizing the morphology of latex particles prior to film formation using cryo-TEM imaging. Panels a and b of Figure 2 show cryo-TEM images of CS-L and CS-H particles, respectively, after removal of water. Cryo-TEM of whole particles obscures clear identification of the two phases due to the thickness contrast from particle curvature convoluting with mass contrast between the acrylic and

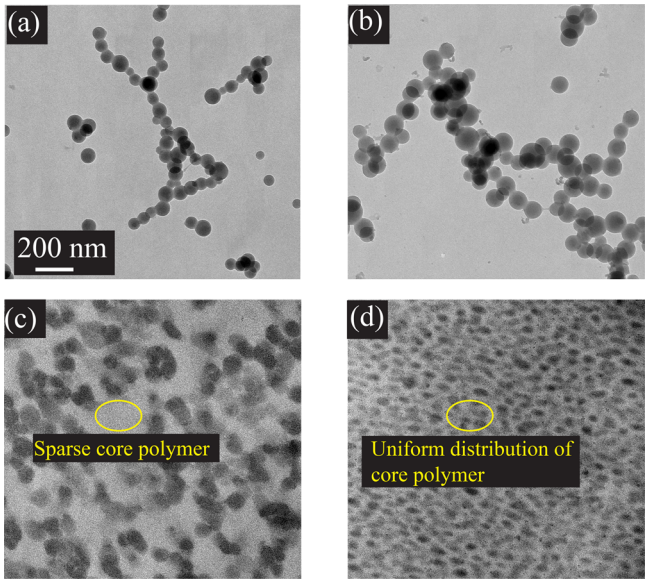

Figure 2. TEM images comparing latex particles CS-L in panels (a) and (c) versus CS-H in panels (b) and (d). Panels (a) and (b) show whole-particle TEM images, whereas panels (c) and (d) show cross sections of cryo-microtomed films (after drying for 2 days). The identification of separate phases is not possible for whole particles, whereas the identification of separate phases is clear for microtomed sections.

acrylic−silicone phases. To overcome this issue, we performed TEM on microtomed particles to enhance the contrast between the different phases.[33,34,77] Here, we image cryo-microtomed sections (≈100 nm thickness) of a film dried for 2 days, rather than embedding whole particles in epoxy followed by microtoming. A 2 day drying time allowed the shell polymer to coalesce into a continuous matrix containing an embedded core polymer, as shown in panels c and d of Figure 2. Because of the mass contrast provided by heavier Si atoms, the acrylic−silicone phase appears darker whereas the acrylic phase appears brighter. Moreover, the core polymer phase is more regularly spaced for CS-H than for CS-L as highlighted in panels c and d of Figure 2, which implies that CS-H has a regular core−shell morphology. CS-L generally shows a slightly occluded core−shell structure,[34] wherein multiple spherical domains of the core polymer are randomly dispersed in the shell.

Following structural characterization of particle morphology, we studied the rheological properties of the shell polymers that ultimately become the matrix within which the core polymers diffuse. Our results show that the dynamics of S-L and S-H are representative of unentangled and entangled polymers from their SAOS master curves obtained using TTS, as shown in Figure 3 for a reference temperature of 27.5 °C. The linear viscoelastic moduli G' and G'' for S-L ($M/M_e \approx 1.39$; $T_g \approx -0.83$ °C) in Figure 3a show a power law scaling of $\omega^{0.5}$ at high frequencies, followed by terminal regime scaling of $G' \sim \omega^2$ and $G'' \sim \omega$, which is consistent with Rouse−Bueche theory for unentangled polymer melts.[81−83] In contrast, G' and G'' for S-H ($M/M_e \approx 19.3$; $T_g \approx 10.65$ °C) in Figure 3b show the transition regime at high frequencies followed by a rubbery plateau regime at lower frequencies, consistent with tube models for entangled polymers.[15−21,84−92] The slow decay of G' in the plateau regime likely arises due to the large dispersity in molecular weight ($Đ \sim 4.54$). The TTS of S-H was performed for temperatures up to 140 °C to avoid thermal

https://doi.org/10.1021/acs.langmuir.2c00855
Langmuir 2022, 38, 11160−11170

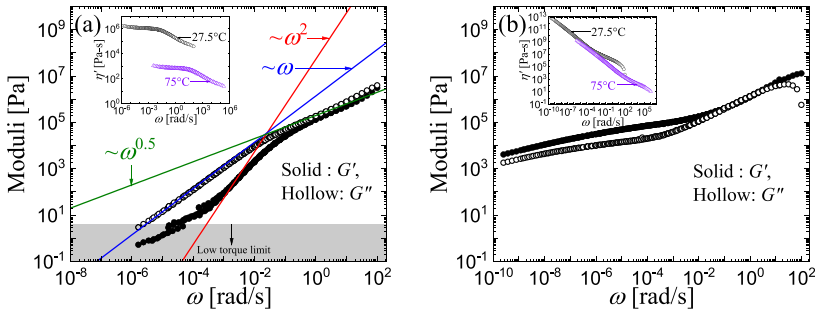

Figure 3. Small-amplitude oscillatory shear (SAOS) master curves for the single-phase latex films obtained using time−temperature superposition (TTS), shown at a reference temperature of 27.5 °C for (a) S-L and (b) S-H. The signatures closely match the expectation for unentangled and entangled polymer melt rheology. The insets show the dynamic viscosity $\eta'(\omega) = G''(\omega)/\omega$ at reference temperatures of 27.5 and 75 °C.

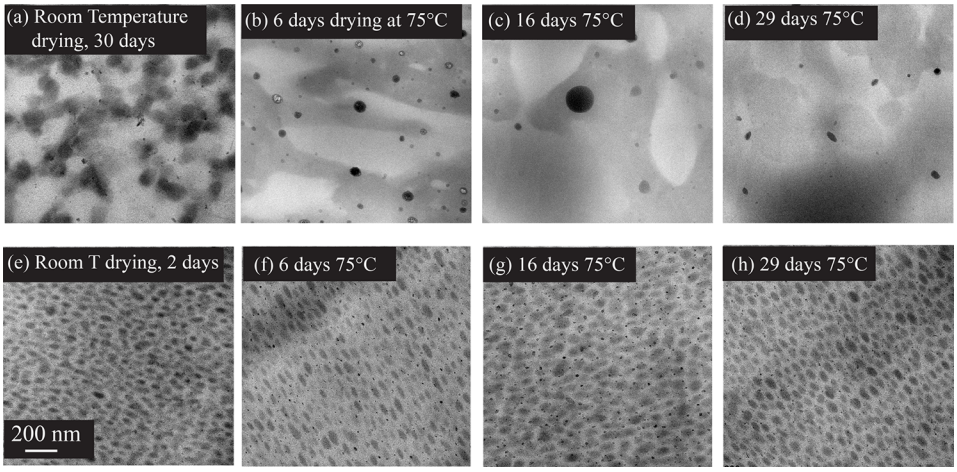

Figure 4. TEM images of cryo-microtomed cross sections of dry films under various conditions for (a)−(d) CS-L and (e)−(h) CS-H. Panels (a) and (e) show images of films dried under ambient conditions at room temperature (≈27.5 °C) for 30 and 2 days, respectively. These states represent the kinetically limited film morphology for ambient condition drying. Films in panels (b)−(d) and (f)−(h) were first dried completely at room temperature, followed by heat aging at 75 °C inside a vacuum oven for the durations indicated on the pictures. Although the film morphology evolves with heat aging for CS-L in panels (b)−(d), it remains unchanged for CS-H in panels (f)−(h).

degradation, and a terminal regime was not observed in that range.

Following rheological characterization of the shell polymer component, we characterized the morphology of multicomponent latex films using TEM imaging of cryo-microtomed cross sections of CS-L films (Figure 4a−d) and CS-H films (Figure 4e−h). Films in panels a and e were dried at room temperature (≈27.5 °C), whereas films in panels b−d and f−h were dried at 75 °C for up to 29 days. For room-temperature drying, both CS-L and CS-H films have similar morphologies of core polymer species embedded in the shell material matrix. In both cases, the core polymer species are immobile in the shell matrix, leading to a simple dry multicomponent latex film morphology (Figure 1) without phase separation. However, for drying at increased high temperatures at 75 °C, CS-L and CS-H show markedly different morphologies. Here, CS-L films show core polymer species coalescence and formation of a biphasic system with co-continuous domains of the two polymers, as soon as after drying for 6 days. The co-continuous domains appear to remain stable and unchanged for longer periods of drying. In contrast, the CS-H film morphology does not change for high-temperature drying and remains the same, showing core polymer species embedded in the shell matrix. On the basis of these observations, polymer coalescence and phase separation in multicomponent latex films can be induced with an unentangled shell polymer and controlled heat aging.

A quantitative analysis was performed to understand the transport behavior in multicomponent latex films using the structural analysis and rheological characterization. The early stage drying process yields a morphology of core polymer species embedded in the shell matrix. Because the core and shell polymeric species are incompatible, it is energetically favorable for the core polymeric species to phase separate in a sea of shell matrix, eventually forming a co-continuous phase within the shell. The viscosity of the shell polymer matrix is a critical property controlling the diffusion of the core species. The viscosity of the shell polymer is determined from rheological experiments (SAOS) as the zero-shear viscosity $\eta_0 \sim \lim_{\omega\to 0} \eta' = \lim_{\omega\to 0} G''/\omega$. The coalescence of spherically shaped core polymeric species occurs on the time scale of diffusion of one core "sphere" from an initial location to a neighboring core polymer "sphere". For a core species sphere of size R, the time to diffuse a distance H between two cores in the shell matrix is estimated via the Stokes−Einstein relation[93] as $\tau_D \approx H^2/2D \approx H^2/2(k_BT/6\pi\eta_0 R)$. The continuum assumption for the shell matrix is valid[93] because the radius of gyration is ≈9 nm[70] for PMMA, which is ∼5 times smaller than the effective size of an isolated spherical core polymer

https://doi.org/10.1021/acs.langmuir.2c00855
Langmuir 2022, 38, 11160−11170

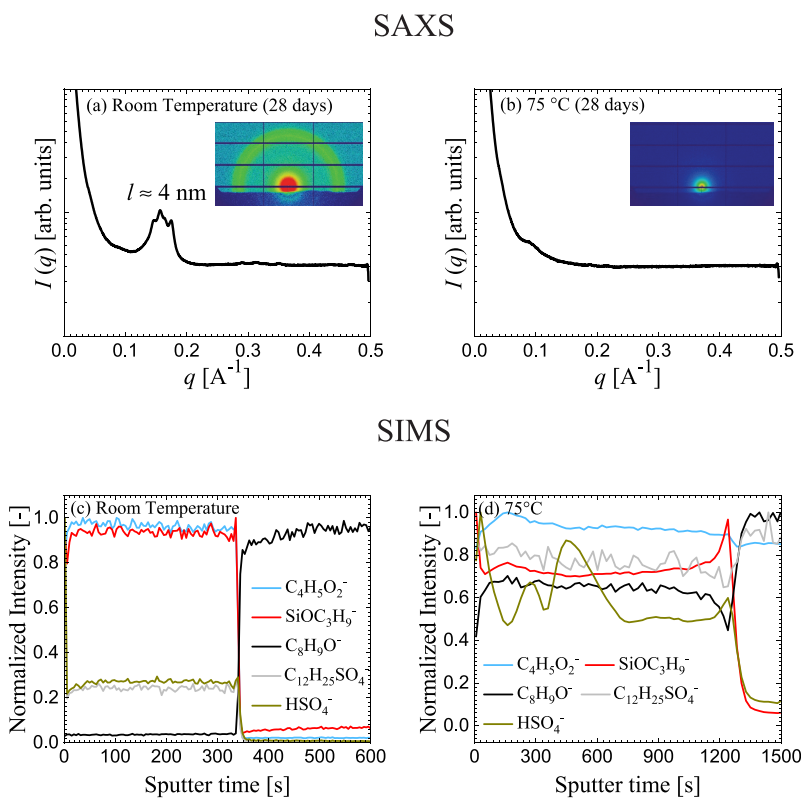

Figure 5. Morphology characterization of CS-L films for room-temperature (≈27.5 °C) and 75 °C drying, each for 28 days via (a)−(b) $I(q)$ SAXS plots and (c)−(d) SIMS depth profiles. SAXS in panels (a) and (b) was done in transmission mode and shows a spherically symmetric feature (inset) of length scale $l = 2\pi/q \approx 4$ nm at room temperature, which disappears at 75 °C. This feature arose due to the surfactant bilayer along the periphery of spherical latex particles at room temperature, which is broken up and dispersed as the core spheres diffuse and coalesce at 75 °C. Interestingly, polymer features corresponding to panels (a) and (d) of Figure 4 cannot be distinguished via SAXS due to insufficient contrast from Si in the core species. Similarly, SIMS in panels (c) and (d) does not show features in agreement with panels (a) and (d) of Figure 4. Rather, the depth profiles of acrylic (corresponding secondary ion, $C_4H_5O_2^-$) and acrylic−silicone ($SiOC_3H_9^-$) species are relatively flat across the film.

particle with a radius of 50 nm. Additional corrections for finite concentration of core species in a shell matrix will not change the order-of-magnitude time scale estimates.[94] From panels c and d of Figure 2, the typical core sphere size (R) and distance between core spheres (H) are ≈50 and ≈100 nm, respectively. The diffusion time scale is therefore $\tau_D \approx 26$ days for core spheres in CS-L, using a zero-shear viscosity of S-L of η_0 (T = 27.5 °C) ≈ 2×10^6 Pa-s, as shown in the inset of Figure 3a. On the basis of this calculation, coalescence and phase separation in CS-L would become prominent after only a few months. These analytical predictions are corroborated in the results shown in Figure 4a, which do not show any significant coalescence of core spheres, even after drying for a month at 27.5 °C. The situation is even more restrictive when the shell material is S-H, where η_0 (T = 27.5 °C) ≫ 10^{13} Pa-s (a lower limit is estimated here because the terminal regime was not achieved for the experimental conditions) as shown in the inset of Figure 3b. The diffusion time scale for core polymers in the high-molecular weight shell polymer is effectively infinite, which manifests as kinetically hindered core polymeric species in the shell matrix for CS-H, as shown in Figure 4e−h.

Increased temperatures can be used to enhance core polymer species diffusion in shell matrices, in part due to the strong dependence of polymer viscosity on temperature. Although the single-component diffusion constants also increase with temperature, the decrease in polymer matrix viscosity plays a more prominent role in enhancing mass transport. When the core−shell latex films are dried at 75 °C, which represents an increase of 47.5 °C from room temperature (≈27.5 °C), the viscosity of S-L decreases to ≈10^3 Pa-s, a 3 order-of-magnitude decrease from 27.5 °C. This enormous decrease in viscosity decreases the characteristic diffusion time scale to $\tau_D \approx 0.026$ days, which suggests enhanced diffusion in CS-L films at 75 °C. These analytical predictions are corroborated by results shown in Figure 4b−d, where the core polymeric species have coalesced to form a co-continuous phase within the shell matrix for drying times of only 6 days. For S-H, even though the viscosity decreases by 4 orders of magnitude, it is still extremely large at 75 °C (>10^9 Pa-s), yielding practically infinite characteristic diffusion time scales for core species, which is corroborated by results shown in Figure 4f−h. Note that the heat aging temperature of 75 °C was selected as a convenient choice for enhancing transport rates. At this temperature, diffusion times decrease from months to hours, thereby enabling the experimental observation of polymer phase separation. In addition, 75 °C is well below the polymer degradation temperature, which ensures minimal or no damage to the sample.

Taken together, the results from structural analysis and rheological characterization indicate that unentangled, or weakly entangled shell polymers can be used to enhance phase separation and potentially promote self-stratification in multicomponent latex films. However, unentangled shell polymers alone may not be sufficient to yield phase separation at lower temperatures. If the viscosity of the shell matrix can be sufficiently decreased by heat aging at slightly increased

https://doi.org/10.1021/acs.langmuir.2c00855
Langmuir 2022, 38, 11160−11170

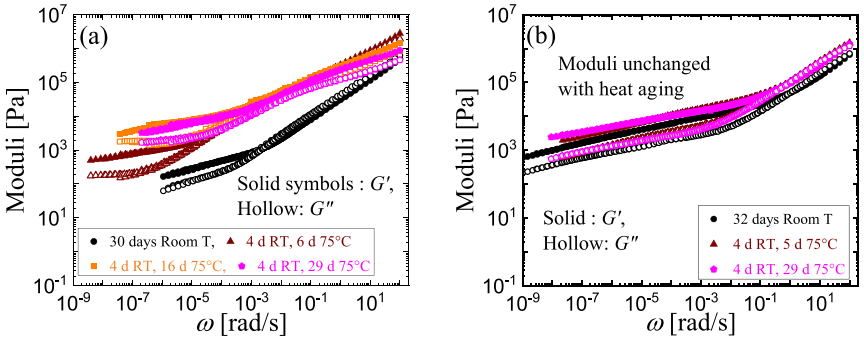

Figure 6. Small-amplitude oscillatory shear (SAOS) master curves for (a) CS-L and (b) CS-H films, obtained using time−temperature superposition (TTS) shown at a reference temperature of 27.5 °C. For panels (a) and (b), data are shown for room-temperature (≈27.5 °C)-dried films and compared with those of films heat aged at 75 °C for various durations (RT = room temperature, d = days).

temperatures, then irreversible phase separation is observed within a few hours or days. The synergistic effect of decreasing the molecular weight of the shell polymer species and heat aging is expected to impart improvements in phase separation for multicomponent latex films as long as the two polymeric species are chemically incompatible. This chemical incompatibility can be assessed a priori, for example, by measuring or estimating the interaction parameter χ.[95−98] However, in systems like ours with multiple polymer species (discussion in section 2), multiple interaction parameters are required to describe the material. On the contrary, a straightforward assessment of chemical incompatibility can be approximately determined using TEM imaging, where incompatible species appear as distinct domains provided that the polymer species have sufficient contrast. In our system, we indeed observe distinct domains of core and shell polymers for both room-temperature and higher-temperature drying as shown in Figure 4. For chemically compatible species, TEM images are expected to show a mixed phase morphology.[33]

A co-continuous phase separation is observed in CS-L system for drying at increased temperatures at 75 °C, as shown in Figure 4b−d, but this process does not yield an ideal phase separation with two distinct layers. The lack of clear stratification into distinct layers likely arises because the core polymer's surface energy is only ≈20% smaller than that of the shell polymer. We hypothesize that a larger surface energy difference would induce phase separation into distinct layers for the heat-aged samples in CS-L.

The success of using TEM of cryo-microtomed films for morphology characterization depends on whether the two phases naturally show contrast. In our case, we observed sufficient contrast between core and shell phases, but this approach might not be generalizable to arbitrary chemistries for core and shell polymers. Staining agents that selectively react with one of the phases can be used to enhance contrast,[99] but in real world applications, one might not deal with model phases, and the contrast might not be available and amenable to enhancement. Given these potential limitations, we sought to determine if SAXS and SIMS could serve as additional methods to characterize multicomponent latex film morphology, and if they yield inferences similar to TEM.

SAXS measurements were used to characterize CS-L films dried at room temperature (≈27.5 °C) and 75 °C, shown as scattering intensity I versus wave-vector q (one-dimensional SAXS profiles) in panels (a) and (b) of Figure 5, with two-dimensional SAXS images shown as insets. The data show correlation peaks centered at approximately $q^* = 0.17$ Å^{-1} indicative of a characteristic correlation length $2\pi/q^*$ of 4 nm present during room-temperature drying, which disappears with high-temperature drying; similar observations were made for S-L films. This correlation length is consistent with the presence of a surfactant bilayer. The surfactant sodium lauryl sulfate has a length of ≈2 nm, resulting in a bilayer with a length of ≈4 nm.[100] The spherical symmetry is likely to arise from the segregation of surfactant bilayers along the periphery of latex particles. For films dried at higher temperatures, the surfactant bilayer structure and preferential segregation are broken as the core spheres begin to diffuse and coalesce under such conditions. Nevertheless, we do not observe any structural features corresponding to core polymeric species (≈100 nm) for room-temperature films or the co-continuous domains (≈1 μm) for heat aging, which are clearly observed in the TEM imaging experiment. We hypothesize that the relatively small fraction of Si (<1 mol %) resulted in a greatly diminished contrast for SAXS experiments.

We next used SIMS for morphological characterization of CS-L films dried at room temperature (≈27.5 °C) and 75 °C, as shown in panels c and d of Figure 5. Here, the intensities of secondary ions were normalized by the maximum observed intensity, and sputter time served as a proxy for film depth. The secondary ions shown originated from acrylic ($C_4H_5O_2^-$), acrylic−silicone ($SiOC_3H_9^-$), mylar substrate ($C_8H_9O^-$), surfactant ($C_{12}H_{25}SO_4^-$), and polymerization initiator or surfactant (HSO_4^-). The film depth corresponds to the point at which the signal arising from the mylar substrate ($C_8H_9O^-$) abruptly increases. For the room-temperature-dried film in Figure 5c, the secondary ions corresponding to acrylic ($C_4H_5O_2^-$) and acrylic−silicone ($SiOC_3H_9^-$) did not show out-of-phase oscillations, which are used for similar structural inferences.[101] The depth profile of films dried at 75 °C shows migration of acrylic−silicone species to air−film and film−substrate interfaces, as shown in Figure 5d. However, the SIMS characterization method cannot capture the details of depth profiles corresponding to the features observed in Figure 4b−d. In fact, the depth profiles of acrylic and acrylic−silicone species were relatively flat, indicating that even under the most controlled conditions, the resolution of SIMS was not adequate to distinguish the morphological details of the film, or the films were not well organized on the length scales interrogated by this experiment.

We next used linear oscillatory shear rheology to characterize the mechanical properties of multicomponent latex films (Figure 6). Shear rheology provides useful insights into film morphology and its dynamic evolution with heat aging. Figure

https://doi.org/10.1021/acs.langmuir.2c00855
Langmuir 2022, 38, 11160−11170

6a shows the master curve from small-amplitude oscillatory shear (SAOS) of CS-L films (at a reference temperature T_{ref} of 27.5 °C) dried at room temperature (≈27.5 °C) and 75 °C. Our results show that the moduli increase with heat aging time, plateauing after heating for ∼16 days. The enhancement of mechanical properties is consistent with the results shown in Figure 4a−d, where the core polymer species domains are observed to separate into well-resolved domains. The coalescence of core polymer species results in an increase in the contiguous domain size of the entangled polymer in the sample, which leads to subsequent enhancements in moduli. In brief, the entangled chains in core domains undergo a transition from isolated regions to co-continuous domains, which results in enhancements in mechanic properties in the material. After heating at 75 °C for 16 days, the moduli show no further increase as phase separation continues. Prior work has reported similar enhancements in the mechanical properties of multicomponent latex films as the morphology changes from discrete core domains to interconnected co-continuous domains.[102−104] In contrast, CS-H films show only the transition regime and the slowly decaying rubbery plateau regime in Figure 6b, characteristic of polydisperse entangled polymer melts, and these moduli remain unchanged with higher-temperature drying. These observations for CS-H are consistent with results shown in Figure 4e−h, where we see an unchanging morphology with spherical core domains effectively immobile in the shell matrix. Our results suggest that bulk rheology is highly sensitive to the morphological changes in multicomponent latex films.

Linear shear rheology data were shifted using TTS for homogeneous species (Figure 3) and for homogeneous and immiscible blends (core and shell species) (Figure 6). The validity of TTS for these cases was confirmed from the temperature-independent van Gurp−Palmen (vGP) plots, as shown in Figures S3−S5. In general, polymer chain length in a homogeneous blend does not significantly influence the temperature dependence of relaxation processes,[79] so TTS is expected to hold for the single-component species shown in Figure 3. The fact that TTS holds reasonably well for blend cases of Figure 6 suggests that the acrylic and acrylic−silicone polymers have nearly the same temperature dependence of their relaxation processes for the temperature range considered.

4. CONCLUSIONS

In this work, we characterize the chemical, morphological, and mechanical properties of multicomponent latex films with a focus on self-stratification behavior. Our results show that the viscosity of the shell matrix significantly dictates the evolution of film morphology. When the viscosity is sufficiently low, the core polymers can diffuse and coalesce within the shell matrix, and phase separation into co-continuous domains is observed as soon as after drying for a few days. The molecular weight of the shell polymer and drying temperature are two important parameters that can be tuned to change or reduce the shell matrix viscosity. Using an unentangled shell polymer coupled with heat aging of films resulted in phase separation, leading to co-continuous domains of the two polymeric species. Our results suggest that entangled shell polymers generally inhibit phase separation, such that the core polymer species remain relatively immobile within the shell matrix even after heat aging for long time periods. Although the unentangled shell polymer coupled with heat aging led to co-continuous domains in latex films, it saturated without proceeding to the idealized distinct layered self-stratification. This is likely due to the relatively small surface energy difference between the polymeric species.

Even though polymer chemistries, molecular weights, and drying conditions can be optimized for improved phase separation and self-stratification in multicomponent latex films, other latex systems can be explored for better and easier self-stratification. Blends of hard latex particles with different sizes have been observed to stratify into various regimes: larger particles at the air−film interface and smaller particles at the air−film interface, depending on the Peclet number *Pe*, which quantifies the relative rate of evaporation to the rate of diffusion, and relative volume fractions of latexes.[24,25,59,60] These ideas can be extended to blends of soft latexes, offering potential advantages in enhancing stratification during the solvent evaporation phase compared to multicomponent latexes where phase separation occurs only after solvent evaporation. In addition, either latex in a blend of different sized latexes can be stratified at the air−film interface, even for small surface energy differences between the two species. For the latex particles studied in this work, we anticipate that the system is dominated by diffusion (low-*Pe* regime). The *Pe* values were estimated as follows. We observed that a 1 mm thick cast solution for rheology discs dried to one-third volume in 3 days, suggesting an evaporation speed $v_E \approx (2/3)/3$ mm/day. Given an initial coating thickness H of ≈100 μm and considering latex particle diffusivity D, *Pe* is given as[61] $Pe \approx Hv_E/D$. Assuming an absolute temperature of 300 K, 100 nm diameter particles, and an initial viscosity of latex similar to that of water, we estimate $Pe \approx 0.06$. Therefore, the latex particles studied under these evaporative conditions are diffusion dominated and expected to be uniformly dispersed in the suspension. We hypothesize that larger diameter latex particles with $Pe \approx 1$ can potentially be stratified at the air−film interface with the smaller latex particles studied in this work underneath them. In this case, the particles could potentially coalesce to form a continuous self-stratified film structure. In addition, the temperature and humidity could be altered to change evaporation rates to obtain different assemblies of latex particles, and subsequently different coalesced film structures.

■ ASSOCIATED CONTENT

Supporting Information

The Supporting Information is available free of charge at https://pubs.acs.org/doi/10.1021/acs.langmuir.2c00855.

Thermogravimetric analysis (TGA) and differential scanning calorimetry (DSC) analysis of dry samples and van Gurp−Palmen (vGP) plots for checking the accuracy of TTS (PDF)

■ AUTHOR INFORMATION

Corresponding Author

Charles M. Schroeder − *Department of Chemical and Biomolecular Engineering, Beckman Institute for Advanced Science and Technology, Department of Materials Science and Engineering, and Materials Research Laboratory, University of Illinois at Urbana-Champaign, Urbana, Illinois 61801, United States;* orcid.org/0000-0001-6023-2274; Email: cms@illinois.edu

https://doi.org/10.1021/acs.langmuir.2c00855
Langmuir 2022, 38, 11160−11170

Authors

Piyush K. Singh − *Department of Chemical and Biomolecular Engineering and Beckman Institute for Advanced Science and Technology, University of Illinois at Urbana-Champaign, Urbana, Illinois 61801, United States;* Present Address: The Dow Chemical Company, Lake Jackson, Texas 77566, United States

Michaeleen L. Pacholski − *The Dow Chemical Company, Collegeville, Pennsylvania 19426-2914, United States*

Junsi Gu − *The Dow Chemical Company, Collegeville, Pennsylvania 19426-2914, United States*

Yoo Kyung Go − *Department of Materials Science and Engineering, University of Illinois at Urbana-Champaign, Urbana, Illinois 61801, United States;* orcid.org/0000-0002-6779-0225

Gaurav Singhal − *Beckman Institute for Advanced Science and Technology and Department of Materials Science and Engineering, University of Illinois at Urbana-Champaign, Urbana, Illinois 61801, United States*

Cecilia Leal − *Beckman Institute for Advanced Science and Technology, Department of Materials Science and Engineering, and Materials Research Laboratory, University of Illinois at Urbana-Champaign, Urbana, Illinois 61801, United States;* orcid.org/0000-0001-5972-508X

Paul V. Braun − *Beckman Institute for Advanced Science and Technology, Department of Materials Science and Engineering, and Materials Research Laboratory, University of Illinois at Urbana-Champaign, Urbana, Illinois 61801, United States;* orcid.org/0000-0003-4079-8160

Kshitish A. Patankar − *The Dow Chemical Company, Midland, Michigan 48667, United States;* orcid.org/0000-0002-3004-427X

Ray Drumright − *The Dow Chemical Company, Midland, Michigan 48667, United States*

Simon A. Rogers − *Department of Chemical and Biomolecular Engineering and Beckman Institute for Advanced Science and Technology, University of Illinois at Urbana-Champaign, Urbana, Illinois 61801, United States*

Complete contact information is available at: https://pubs.acs.org/10.1021/acs.langmuir.2c00855

Notes

The authors declare no competing financial interest.

■ ACKNOWLEDGMENTS

The authors acknowledge the Dow University Partnership Initiative (UPI Program) for financial support. The authors thank Luke Yu from the University of Illinois at Urbana-Champaign for useful insights on modeling. Insightful discussions with Hyeonmin Jeong and Charles Sing (Illinois) and Praveen Agarwal, Paul Mwasame, Sipei Zhang, Sean Tang, and Melinda Einsla (Dow) are gratefully acknowledged. The authors thank Hilda Buss (Dow) for chemical synthesis. This research was carried out in part in the Materials Research Laboratory Central Research Facilities, University of Illinois, where the support of research scientists, particularly, Roddel Remy, Timothy Spila, and Mohammad Amdad Ali, is greatly appreciated. Synchrotron X-ray experiments were conducted at beamline 12-ID-B at the Advanced Photon Source (APS), Argonne National Laboratory. Use of APS was supported by the U.S. Department of Energy (DOE), Office of Science, Office of Basic Energy Sciences, under Contract DE-AC02-06CH11357. The SAXS characterization experiments were supported by the National Science Foundation under Grant DMR-1554435.

■ REFERENCES

(1) Karim, A.; Mansour, A.; Felcher, G.; Russell, T. Short-time relaxation at polymeric interfaces. *Phys. Rev. B* **1990**, *42* (10), 6846.

(2) Kim, K. D.; Sperling, L.; Klein, A.; Hammouda, B. Reptation time, temperature, and cosurfactant effects on the molecular interdiffusion rate during polystyrene latex film formation. *Macromolecules* **1994**, *27* (23), 6841−6850.

(3) Russell, T.; Deline, V.; Dozier, W.; Felcher, G.; Agrawal, G.; Wool, R.; Mays, J. Direct observation of reptation at polymer interfaces. *Nature* **1993**, *365* (6443), 235−237.

(4) Pekcan, O.; Winnik, M. A.; Croucher, M. D. Fluorescence studies of coalescence and film formation in poly (methyl methacrylate) nonaqueous dispersion particles. *Macromolecules* **1990**, *23* (10), 2673−2678.

(5) Wang, Y.; Winnik, M. A. Effect of a coalescing aid on polymer diffusion in latex films. *Macromolecules* **1990**, *23* (21), 4731−4732.

(6) Wang, Y.; Winnik, M. A. Polymer diffusion across interfaces in latex films. *J. Phys. Chem.* **1993**, *97* (11), 2507−2515.

(7) Wang, Y.; Zhao, C. L.; Winnik, M. A. Molecular diffusion and latex film formation: an analysis of direct nonradiative energy transfer experiments. *J. Chem. Phys.* **1991**, *95* (3), 2143−2153.

(8) Winnik, M. A.; Wang, Y.; Haley, F. Latex film formation at the molecular level: The effect of coalescing aids on polymer diffusion. *J. Coat. Technol.* **1992**, *64* (811), 51−61.

(9) Zhao, C. L.; Wang, Y.; Hruska, Z.; Winnik, M. A. Molecular aspects of latex film formation: an energy-transfer study. *Macromolecules* **1990**, *23* (18), 4082−4087.

(10) Keddie, J.; Routh, A. F. *Fundamentals of latex film formation: processes and properties*; Springer Science & Business Media, 2010.

(11) Keddie, J. L. Film formation of latex. *Materials Science and Engineering: R: Reports* **1997**, *21* (3), 101−170.

(12) Winnik, M. A. Latex film formation. *Current opinion in colloid & interface science* **1997**, *2* (2), 192−199.

(13) Dobler, F.; Holl, Y. Mechanisms of latex film formation. *Trends Polym. Sci.* **1996**, *5* (4), 145−151.

(14) Steward, P.; Hearn, J.; Wilkinson, M. An overview of polymer latex film formation and properties. *Advances in colloid and interface science* **2000**, *86* (3), 195−267.

(15) Dealy, J. M.; Larson, R. G. *Structure and Rheology of Molten Polymers: From Structure to Flow Behavior and Back Again*; Hanser Publishers: Munich, 2006; Chapter 6.

(16) Doi, M.; Edwards, S. Dynamics of concentrated polymer systems. Part 1.—Brownian motion in the equilibrium state. *Journal of the Chemical Society, Faraday Transactions 2: Molecular and Chemical Physics* **1978**, *74*, 1789−1801.

(17) Doi, M.; Edwards, S. Dynamics of concentrated polymer systems. Part 2.—Molecular motion under flow. *Journal of the Chemical Society, Faraday Transactions 2: Molecular and Chemical Physics* **1978**, *74*, 1802−1817.

(18) Doi, M.; Edwards, S. Dynamics of concentrated polymer systems. Part 3.—The constitutive equation. *Journal of the Chemical Society, Faraday Transactions 2: Molecular and Chemical Physics* **1978**, *74*, 1818−1832.

(19) Doi, M.; Edwards, S. Dynamics of concentrated polymer systems. Part 4.—Rheological properties. *Journal of the Chemical Society, Faraday Transactions 2: Molecular and Chemical Physics* **1979**, *75*, 38−54.

(20) Doi, M.; Edwards, S. F. *The theory of polymer dynamics*; Oxford University Press: New York, 1986.

(21) Pearson, D. S.; Rochefort, W. E. Behavior of concentrated polystyrene solutions in large-amplitude oscillating shear fields. *J. Polym. Sci., Polym. Phys. Ed.* **1982**, *20* (1), 83−98.

(22) Guyot, A.; Landfester, K.; Schork, F. J.; Wang, C. Hybrid polymer latexes. *Prog. Polym. Sci.* **2007**, *32* (12), 1439−1461.

(23) Wang, C.; Chu, F.; Graillat, C.; Guyot, A.; Gauthier, C.; Chapel, J. Hybrid polymer latexes: acrylics−polyurethane from miniemulsion polymerization: properties of hybrid latexes versus blends. *Polymer* **2005**, *46* (4), 1113−1124.
(24) Zhou, J.; Jiang, Y.; Doi, M. Cross interaction drives stratification in drying film of binary colloidal mixtures. *Physical review letters* **2017**, *118* (10), 108002.
(25) Dong, Y.; Busatto, N.; Roth, P. J.; Martin-Fabiani, I. Colloidal assembly of polydisperse particle blends during drying. *Soft Matter* **2020**, *16* (36), 8453−8461.
(26) Schulz, M.; Keddie, J. A critical and quantitative review of the stratification of particles during the drying of colloidal films. *Soft Matter* **2018**, *14* (30), 6181−6197.
(27) Toussaint, A. Self-stratifying coatings for plastic substrates (Brite euram project RI 1B 0246 C (H)). *Prog. Org. Coat.* **1996**, *28* (3), 183−195.
(28) Fei, G.; Wang, H.; Li, X.; Mou, J. Rheology, mechanical, and thermal properties of core−shell silicon-acrylic copolymer emulsion films and its application on surface sizing: role of silane coupling agent. *Polym. Bull.* **2011**, *67* (6), 1017.
(29) Kan, C. Y.; Kong, X. Z.; Yuan, Q.; Liu, D. S. Morphological prediction and its application to the synthesis of polyacrylate/polysiloxane core/shell latex particles. *J. Appl. Polym. Sci.* **2001**, *80* (12), 2251−2258.
(30) Lin, M.; Chu, F.; Guyot, A.; Putaux, J.-L.; Bourgeat-Lami, E. Silicone−polyacrylate composite latex particles. Particles formation and film properties. *Polymer* **2005**, *46* (4), 1331−1337.
(31) Mackulin, P. J.; Krafcik, R. B.; Borns, B. M.; Doshi, J. K.; Zhao, W. Self-stratifying coatings. US 9000060 B1, 2015.
(32) Liu, Z.; Zhao, Y.; Zhou, J.; Yuan, X. Synthesis and characterization of core−shell polyacrylate latex containing fluorine/silicone in the shell and the self-stratification film. *Colloid Polym. Sci.* **2012**, *290* (3), 203−211.
(33) Stubbs, J. M.; Sundberg, D. C. The dynamics of morphology development in multiphase latex particles. *Prog. Org. Coat.* **2008**, *61* (2−4), 156−165.
(34) Stubbs, J. M.; Sundberg, D. C. Core-shell and other multiphase latex particles—confirming their morphologies and relating those to synthesis variables. *Journal of Coatings Technology and Research* **2008**, *5* (2), 169−180.
(35) Monovoukas, Y.; Gast, A. P. The experimental phase diagram of charged colloidal suspensions. *J. Colloid Interface Sci.* **1989**, *128* (2), 533−548.
(36) Pusey, P.; Zaccarelli, E.; Valeriani, C.; Sanz, E.; Poon, W. C.; Cates, M. E. Hard spheres: crystallization and glass formation. *Philosophical Transactions of the Royal Society A: Mathematical, Physical and Engineering Sciences* **2009**, *367* (1909), 4993−5011.
(37) Pusey, P. N.; Van Megen, W. Phase behaviour of concentrated suspensions of nearly hard colloidal spheres. *Nature* **1986**, *320* (6060), 340−342.
(38) Bareigts, G.; Kiatkirakajorn, P.-C.; Li, J.; Botet, R.; Sztucki, M.; Cabane, B.; Goehring, L.; Labbez, C. Packing polydisperse colloids into crystals: when charge-dispersity matters. *Phys. Rev. Lett.* **2020**, *124* (5), 058003.
(39) Cabane, B.; Li, J.; Artzner, F.; Botet, R.; Labbez, C.; Bareigts, G.; Sztucki, M.; Goehring, L. Hiding in plain view: colloidal self-assembly from polydisperse populations. *Phys. Rev. Lett.* **2016**, *116* (20), 208001.
(40) Fasolo, M.; Sollich, P. Fractionation effects in phase equilibria of polydisperse hard-sphere colloids. *Phys. Rev. E* **2004**, *70* (4), 041410.
(41) Botet, R.; Cabane, B.; Goehring, L.; Li, J.; Artzner, F. How do polydisperse repulsive colloids crystallize? *Faraday Discuss.* **2016**, *186*, 229−240.
(42) Banik, M.; Sett, S.; Bakli, C.; Raychaudhuri, A. K.; Chakraborty, S.; Mukherjee, R. Substrate wettability guided oriented self assembly of Janus particles. *Sci. Rep.* **2021**, *11* (1), 1182.
(43) Banik, M.; Bhandaru, N.; Mukherjee, R. Transfer printing of colloidal crystals based on UV mediated degradation of a polymer thin film. *Chem. Commun.* **2018**, *54* (28), 3484−3487.
(44) Amos, R. M.; Rarity, J. G.; Tapster, P. R.; Shepherd, T. J.; Kitson, S. C. Fabrication of large-area face-centered-cubic hard-sphere colloidal crystals by shear alignment. *Phys. Rev. E* **2000**, *61* (3), 2929−2935.
(45) Cecchini, M. P.; Turek, V. A.; Paget, J.; Kornyshev, A. A.; Edel, J. B. Self-assembled nanoparticle arrays for multiphase trace analyte detection. *Nat. Mater.* **2013**, *12* (2), 165−171.
(46) Christie, D.; Lombardi, J.; Kretzschmar, I. Two-dimensional array of silica particles as a SERS substrate. *J. Phys. Chem. C* **2014**, *118* (17), 9114−9118.
(47) Cong, H.; Yu, B.; Tang, J.; Li, Z.; Liu, X. Current status and future developments in preparation and application of colloidal crystals. *Chem. Soc. Rev.* **2013**, *42* (19), 7774−7800.
(48) Deckman, H. W.; Dunsmuir, J. H. Natural lithography. *Appl. Phys. Lett.* **1982**, *41* (4), 377−379.
(49) Deckman, H. W.; Dunsmuir, J. H.; Garoff, S.; McHenry, J. A.; Peiffer, D. G. Macromolecular self-organized assemblies. *Journal of Vacuum Science & Technology B: Microelectronics Processing and Phenomena* **1988**, *6* (1), 333−336.
(50) Denkov, N. D.; Velev, O. D.; Kralchevsky, P. A.; Ivanov, I. B.; Yoshimura, H.; Nagayama, K. Two-dimensional crystallization. *Nature* **1993**, *361* (6407), 26−26.
(51) Haynes, C. L.; Van Duyne, R. P. Nanosphere Lithography: A Versatile Nanofabrication Tool for Studies of Size-Dependent Nanoparticle Optics. *J. Phys. Chem. B* **2001**, *105* (24), 5599−5611.
(52) Karg, M.; König, T. A. F.; Retsch, M.; Stelling, C.; Reichstein, P. M.; Honold, T.; Thelakkat, M.; Fery, A. Colloidal self-assembly concepts for light management in photovoltaics. *Mater. Today* **2015**, *18* (4), 185−205.
(53) Kruglova, O.; Demeyer, P.-J.; Zhong, K.; Zhou, Y.; Clays, K. Wonders of colloidal assembly. *Soft Matter* **2013**, *9* (38), 9072−9087.
(54) Meng, K.; Gao, S.; Wu, L.; Wang, G.; Liu, X.; Chen, G.; Liu, Z.; Chen, G. Two-Dimensional Organic−Inorganic Hybrid Perovskite Photonic Films. *Nano Lett.* **2016**, *16* (7), 4166−4173.
(55) Mihi, A.; Ocaña, M.; Míguez, H. Oriented Colloidal-Crystal Thin Films by Spin-Coating Microspheres Dispersed in Volatile Media. *Adv. Mater.* **2006**, *18* (17), 2244−2249.
(56) Pieranski, P.; Strzelecki, L.; Pansu, B. Thin Colloidal Crystals. *Phys. Rev. Lett.* **1983**, *50* (12), 900−903.
(57) Shiu, J.-Y.; Kuo, C.-W.; Chen, P.; Mou, C.-Y. Fabrication of Tunable Superhydrophobic Surfaces by Nanosphere Lithography. *Chem. Mater.* **2004**, *16* (4), 561−564.
(58) Das, A.; Dey, A. B.; Chattopadhyay, S.; De, G.; Sanyal, M. K.; Mukherjee, R. Nanoparticle Induced Morphology Modulation in Spin Coated PS/PMMA Blend Thin Films. *Langmuir* **2020**, *36* (50), 15270−15282.
(59) Schulz, M.; Crean, C.; Brinkhuis, R.; Sear, R.; Keddie, J. Determination of parameters for self-stratification in bimodal colloidal coatings using Raman depth profiling. *Prog. Org. Coat.* **2021**, *157*, 106272.
(60) Fortini, A.; Martín-Fabiani, I.; De La Haye, J. L.; Dugas, P.-Y.; Lansalot, M.; D'agosto, F.; Bourgeat-Lami, E.; Keddie, J. L.; Sear, R. P. Dynamic stratification in drying films of colloidal mixtures. *Phys. Rev. Lett.* **2016**, *116* (11), 118301.
(61) Howard, M. P.; Nikoubashman, A.; Panagiotopoulos, A. Z. Stratification dynamics in drying colloidal mixtures. *Langmuir* **2017**, *33* (15), 3685−3693.
(62) Rees-Zimmerman, C. R.; Routh, A. F. Stratification in drying films: a diffusion−diffusiophoresis model. *J. Fluid Mech.* **2021**, *928*, A15.
(63) Trueman, R.; Lago Domingues, E.; Emmett, S.; Murray, M.; Routh, A. Auto-stratification in drying colloidal dispersions: A diffusive model. *J. Colloid Interface Sci.* **2012**, *377* (1), 207−212.
(64) Atmuri, A. K.; Bhatia, S. R.; Routh, A. F. Autostratification in drying colloidal dispersions: Effect of particle interactions. *Langmuir* **2012**, *28* (5), 2652−2658.

https://doi.org/10.1021/acs.langmuir.2c00855
Langmuir 2022, 38, 11160−11170

(65) Nikiforow, I.; Adams, J. r.; König, A. M.; Langhoff, A.; Pohl, K.; Turshatov, A.; Johannsmann, D. Self-stratification during film formation from latex blends driven by differences in collective diffusivity. *Langmuir* **2010**, *26* (16), 13162−13167.
(66) Carr, A. J.; Liu, W.; Yager, K. G.; Routh, A. F.; Bhatia, S. R. Evidence of stratification in binary colloidal films from microbeam X-ray scattering: Toward optimizing the evaporative assembly processes for coatings. *ACS Applied Nano Materials* **2018**, *1* (8), 4211−4217.
(67) Liu, W.; Carr, A. J.; Yager, K. G.; Routh, A. F.; Bhatia, S. R. Sandwich layering in binary nanoparticle films and effect of size ratio on stratification behavior. *J. Colloid Interface Sci.* **2019**, *538*, 209−217.
(68) Liu, X.; Liu, W.; Carr, A. J.; Santiago Vazquez, D.; Nykypanchuk, D.; Majewski, P. W.; Routh, A. F.; Bhatia, S. R. Stratification during evaporative assembly of multicomponent nanoparticle films. *J. Colloid Interface Sci.* **2018**, *515*, 70−77.
(69) Mark, J. E. *Physical properties of polymers handbook*, 2nd ed.; Springer, 2007; Chapter 59.
(70) Fetters, L. J.; Lohse, D. J.; Milner, S. T.; Graessley, W. W. Packing length influence in linear polymer melts on the entanglement, critical, and reptation molecular weights. *Macromolecules* **1999**, *32* (20), 6847−6851.
(71) Lovell, P. A.; El-Aasser, M. S. *Emulsion polymerization and emulsion polymers*; Wiley, 1997.
(72) Sundberg, D. C.; Casassa, A. P.; Pantazopoulos, J.; Muscato, M. R.; Kronberg, B.; Berg, J. Morphology development of polymeric microparticles in aqueous dispersions. I. Thermodynamic considerations. *J. Appl. Polym. Sci.* **1990**, *41* (7−8), 1425−1442.
(73) Chen, Y. C.; Dimonie, V.; El-Aasser, M. S. Interfacial phenomena controlling particle morphology of composite latexes. *J. Appl. Polym. Sci.* **1991**, *42* (4), 1049−1063.
(74) Gonzalez-Ortiz, L. J.; Asua, J. M. Development of particle morphology in emulsion polymerization. 1. Cluster dynamics. *Macromolecules* **1995**, *28* (9), 3135−3145.
(75) González-Ortiz, L. J.; Asua, J. M. Development of particle morphology in emulsion polymerization. 3. Cluster nucleation and dynamics in polymerizing systems. *Macromolecules* **1996**, *29* (13), 4520−4527.
(76) González-Ortiz, L. J.; Asua, J. M. Development of particle morphology in emulsion polymerization. 2. Cluster dynamics in reacting systems. *Macromolecules* **1996**, *29* (1), 383−389.
(77) Stubbs, J. M.; Sundberg, D. C. A round robin study for the characterization of latex particle morphology—multiple analytical techniques to probe specific structural features. *Polymer* **2005**, *46* (4), 1125−1138.
(78) Ferry, J. D. *Viscoelastic properties of polymers*; John Wiley & Sons: New York, 1980.
(79) Van Gurp, M.; Palmen, J. Time-temperature superposition for polymeric blends. *Rheol. Bull.* **1998**, *67* (1), 5−8.
(80) Dealy, J.; Plazek, D. Time-temperature superposition—a users guide. *Rheol. Bull.* **2009**, *78* (2), 16−31.
(81) Bueche, F. Viscosity, self-diffusion, and allied effects in solid polymers. *J. Chem. Phys.* **1952**, *20* (12), 1959−1964.
(82) Dealy, J. M.; Larson, R. G. *Structure and rheology of molten polymers: from structure to flow behavior and back again*; Hanser Publications: Munich, 2006.
(83) Rouse, P. E., Jr A theory of the linear viscoelastic properties of dilute solutions of coiling polymers. *J. Chem. Phys.* **1953**, *21* (7), 1272−1280.
(84) Doi, M. Explanation for the 3.4 power law of viscosity of polymeric liquids on the basis of the tube model. *J. Polym. Sci. (Hoboken, NJ, U. S.)* **1981**, *19* (5), 265−273.
(85) Doi, M. Explanation for the 3.4-power law for viscosity of polymeric liquids on the basis of the tube model. *J. Polym. Sci., Polym. Phys. Ed.* **1983**, *21* (5), 667−684.
(86) Benallal, A.; Marin, G.; Montfort, J.; Derail, C. Linear viscoelasticity revisited: the relaxation function of monodisperse polymer melts. *Macromolecules* **1993**, *26* (26), 7229−7235.
(87) McLeish, T. Tube theory of entangled polymer dynamics. *Advances in physics* **2002**, *51* (6), 1379−1527.
(88) Watanabe, H. Viscoelasticity and dynamics of entangled polymers. *Prog. Polym. Sci.* **1999**, *24* (9), 1253−1403.
(89) Likhtman, A. E.; McLeish, T. C. Quantitative theory for linear dynamics of linear entangled polymers. *Macromolecules* **2002**, *35* (16), 6332−6343.
(90) Milner, S.; McLeish, T. Reptation and contour-length fluctuations in melts of linear polymers. *Phys. Rev. Lett.* **1998**, *81* (3), 725.
(91) Pattamaprom, C.; Larson, R. G. Predicting the linear viscoelastic properties of monodisperse and polydisperse polystyrenes and polyethylenes. *Rheol. Acta* **2001**, *40* (6), 516−532.
(92) Pattamaprom, C.; Larson, R. G.; Van Dyke, T. J. Quantitative predictions of linear viscoelastic rheological properties of entangled polymers. *Rheol. Acta* **2000**, *39* (6), 517−531.
(93) Deen, W. M. *Analysis of transport phenomena*; Oxford University Press: New York, 1998; Vol. 2.
(94) Batchelor, G. The effect of Brownian motion on the bulk stress in a suspension of spherical particles. *Journal of fluid mechanics* **1977**, *83* (1), 97−117.
(95) Flory, P. J. Thermodynamics of high polymer solutions. *J. Chem. Phys.* **1941**, *9* (8), 660−660.
(96) Hiemenz, P. C.; Lodge, T. P. *Polymer chemistry*, 2nd ed.; CRC Press: Boca Raton, FL, 2007.
(97) Huggins, M. L. Solutions of long chain compounds. *J. Chem. Phys.* **1941**, *9* (5), 440−440.
(98) Scott, R. L. Thermodynamics of high polymer solutions. VI. The compatibility of copolymers. *J. Polym. Sci.* **1952**, *9* (5), 423−432.
(99) Domingues Dos Santos, F.; Fabre, P.; Drujon, X.; Meunier, G.; Leibler, L. Films from soft-core/hard-shell hydrophobic latexes: Structure and thermomechanical properties. *J. Polym. Sci., Part B: Polym. Phys.* **2000**, *38* (23), 2989−3000.
(100) Šegota, S.; Težak, Đ.; Talmon, Y. New Catanionic Mixtures of Didodecyldimethylammonium Bromide/Sodium Dodecylbenzene sulfonate/Water with Special Reference to Spontaneous Formation of Vesicles. II. Size and Shape Analysis by SAXS, Light Scattering, Cryo-TEM, and Light Microscopy. *Soft Mater.* **2005**, *3* (2−3), 51−69.
(101) Pacholski, M. L.; Qu, Z.; Ouyang, W.; Zheng, Z.; Wang, R. Particle-based chemical oscillation as a function of depth in latex films using gas cluster ion beam secondary ion mass spectrometry profiling. *J. Vac. Sci. Technol., B: Nanotechnol. Microelectron.: Mater., Process., Meas., Phenom.* **2018**, *36* (3), n/a.
(102) O'Connor, K. M.; Tsaur, S. L. Phase rearrangement in two-stage emulsion polymers of butyl acrylate and styrene: Mechanical properties. *J. Appl. Polym. Sci.* **1987**, *33* (6), 2007−2027.
(103) Hidalgo, M.; Cavaille, J.; Guillot, J.; Guyot, A.; Perez, J.; Vassoille, R. Polystyrene (1)/poly (butyl acrylate/amide type functional monomer)(2) two-stage emulsion polymers. Synthesis and thermomechanical properties of latex films. *J. Polym. Sci., Part B: Polym. Phys.* **1995**, *33* (11), 1559−1572.
(104) Cavaillé, J.; Vassoille, R.; Thollet, G.; Rios, L.; Pichot, C. Structural morphology of poly (styrene)-poly (butyl acrylate) polymer-polymer composites studied by dynamic mechanical measurements. *Colloid and polymer science* **1991**, *269* (3), 248−258.

https://doi.org/10.1021/acs.langmuir.2c00855
Langmuir 2022, 38, 11160−11170